Two New μ-Azido Nickel(II) Uniform Chains: Syntheses, Structures, and Magneto–Structural Correlations

Albert Escuer,*,† Ramon Vicente,† Joan Ribas,† M. Salah El Fallah,† Xavier Solans,‡ and M. Font-Bardía‡

Departament de Química Inorgànica, Universitat de Barcelona, Diagonal 647, 08028-Barcelona, Spain, and Departament de Cristal.lografia i Mineralogia, Universitat de Barcelona, Martí Franqués s/n 08028-Barcelona, Spain

Received December 16, 1992

Two new monodimensional (μ-azido)nickel(II) complexes of formulas *catena*-(μ-N_3)[Ni(232-tet)](ClO_4) (**1**) and *catena*-(μ-N_3)[Ni(323-tet)](ClO_4) (**2**) have been synthesized and characterized. 232-tet and 323-tet are the tetraamines *N*,*N*′-bis(2-aminoethyl)-1,3-propanediamine and *N*,*N*′-bis(3-aminopropyl)-1,2-ethanediamine, respectively. The crystal structures of **1** and **2** have been solved. The complex $[C_7H_{20}N_7Ni]_n(ClO_4)_n$ (**1**) crystallizes in the monoclinic system, space group $P2_1/a$, with fw = 360.44, a = 11.806(3) Å, b = 13.154(3) Å, c = 9.598(2) Å, β = 97.90(2)°, V = 1476(1) Å^3, Z = 4, R = 0.045, and R_w = 0.055. The complex $[C_8H_{22}N_7Ni]_n(ClO_4)_n$ (**2**) crystallizes in the orthorhombic system, space group *Pbca*, with fw = 374.47, a = 17.151(2) Å, b = 16.267(2) Å, c = 11.478(2) Å, V = 3203(1) Å^3, Z = 8, R = 0.049, and R_w = 0.058. In both compounds the nickel atoms are placed in an octahedral environment with the μ-azido groups in *trans* positions. The magnetic properties of these compounds have been studied. The thermal variation of the molar susceptibility is typical of an antiferromagnetically coupled nickel(II) uniform chain displaying Haldane gap behavior. Using the Hamiltonian $H = -J\sum S_i S_{i+1}$, the J values obtained were –26.9 and –62.7 cm^{-1} for **1** and **2**, respectively. Magneto–structural correlations have been obtained in a series of analogous systems, using extended Hückel calculations.

Introduction

Monodimensional nickel(II) compounds are relatively scarce, and the bridging ligands used to generate this kind of system to date are carboxylato derivatives,[1] oxalato and related ligands,[2] nitrito,[3] halides,[4] cyanide,[5] and thiocyanato.[6] The azide ion is the last ligand to be incorporated into this group of bridging ligands. It potentially can allow the synthesis of 1-D derivatives[7,8] with interesting magnetic properties. As is well-known, the azido ligand stabilizes either end-on or end-to-end coordination modes when it links two nickel(II) centers, giving ferro-[9–11] or antiferromagnetic[12–14] compounds, respectively. On the other hand, the end-to-end coordination shows different bond parameters in all compounds synthesized to date as a consequence of the free coordination of a linear triatomic molecule without steric hindrance between two metallic ions. Consequently, the end-to-end azido ligand gives a wide range of antiferromagnetic interactions (literature data show, for example, $-J$ coupling constants in the range 24–90 cm^{-1} for dinuclear [NiNi] systems[12–14]). Magneto–structural correlations have not been reported.

In recent papers, we reported the synthesis of two monodimensional nickel(II) compounds bridged by azido ligands: *catena*-(μ-N_3)$_3$[Ni_2(dpt)$_2$](ClO_4) (dpt = bis(3-aminopropyl)amine), a structural and magnetic alternating $(-N_3-NiL-(N_3)_2-NiL-)_n$ chain,[7] and *catena*-(μ-N_3)[Ni(cyclam)](ClO_4)·H_2O (cyclam = 1,4,8,11-tetraazacyclotetradecane), a uniform $(-N_3-NiL-)_n$ chain.[8] The preparation of *catena*-(μ-N_3)[Ni(cyclam)](ClO_4)·H_2O is an example of a general synthetic method to obtain 1-D nickel(II)–azido systems, tailored from *trans* tetraamine complexes of nickel(II) ion. Following this synthetic pathway, we prepared two new compounds: *catena*-(μ-N_3)[Ni(232-tet)](ClO_4), where 232-tet is the tetraamine *N*,*N*′-bis(2-aminoethyl)-1,3-propanediamine, and *catena*-(μ-N_3)[Ni(323-tet)](ClO_4), where 323-tet is the tetraamine *N*,*N*′-bis(3-aminopropyl)-1,2-ethanediamine. These compounds present the azido groups in an end-to-end fashion in a *trans* arrangement around the nickel atom, as already found for *catena*-(μ-N_3)[Ni(cyclam)](ClO_4)·H_2O. The magnetic behaviors of **1** and **2** are similar, showing strong antiferromagnetic coupling, as previously found for *catena*-(μ-N_3)[Ni(cyclam)]-(ClO_4)·H_2O,[8] but the J parameters are very different for both compounds: –26.9 and –62.7 cm^{-1} for **1** and **2**, respectively. With the aim of correlating this magnetic behavior with structural parameters, extended Hückel MO calculations have been performed on the structurally characterized 1-D complexes in an attempt to explain the variation in the magnetic coupling as a function of the bond parameters.

Experimental Section

Synthesis. Caution! Perchlorate salts of metal complexes with organic ligands are potentially explosive. Only a small amount of material should be prepared, and it should be handled with caution.

To a concentrated aqueous solution of 2 mmol of 232-tet or 323-tet and 2 mmol of $Ni(ClO_4)_2$·$6H_2O$ was added 2 mmol of NaN_3 dissolved

† Department of Inorganic Chemistry.
‡ Department of Crystallography.

(1) Endres, H. *Z. Anorg. Allg. Chem.* **1984**, *513*, 78. Coronado, E.; Drillon, M.; Fuertes, A.; Beltran, D.; Mosset, A.; Galy, J. *J. Am. Chem. Soc.* **1986**, *108*, 900.
(2) Soules, R.; Dahan, F.; Laurent, J.-P.; Castan, P. *J. Chem. Soc., Dalton Trans.* **1988**, 587.
(3) Meyer, A.; Gleizes, A.; Girerd, J.-J.; Verdaguer, M.; Kahn, O. *Inorg. Chem.* **1982**, *21*, 1729.
(4) Bkouche-Waksman, I.; L'Haridom, P. *Bull. Soc. Chim. Fr.* **1983**, *25*, 30.
(5) Hasegawa, T.; Nishikiori, S.; Iwamoto, T. *Chem. Lett.* **1985**, 1659.
(6) Turpeinen, U.; Ahlgren, M. *Finn. Chem. Lett.* **1977**, *75*, 274.
(7) Vicente, R.; Escuer, A.; Ribas, J.; Solans, X. *Inorg. Chem.* **1992**, *31*, 1726.
(8) Escuer, A.; Vicente, R.; Ribas, J.; Salah El Fallah, M.; Solans, X. *Inorg. Chem.* **1993**, *32*, 1033.
(9) Arriortua, M. I.; Cortes, R.; Lezama, L.; Rojo, T.; Solans, X.; Font-Bardia, M. *Inorg. Chim. Acta* **1990**, *174*, 263.
(10) Escuer, A.; Vicente, R.; Ribas, J. *J. Magn. Magn. Mater.* **1992**, *110*, 181.
(11) Cortes, R.; Ruiz de Larramendi, J. I.; Lezama, L.; Rojo, T.; Urtiaga, K.; Arriortua, M. I. *J. Chem. Soc., Dalton Trans.* **1992**, 2723.
(12) Wagner, F.; Mocella, M. T.; D'Aniello, M. J.; Wang, A. H. J.; Barefield, E. K. *J. Am. Chem. Soc.* **1974**, *96*, 2625.
(13) Pierpont, C. G.; Hendrickson, D. N.; Duggan, D. M.; Wagner, F.; Barefield, E. K. *Inorg. Chem.* **1975**, *14*, 604.
(14) Chaudhuri, P.; Guttmann, M.; Ventur, D.; Wieghardt, K.; Nuber, B.; Weiss, J. *J. Chem. Soc., Chem. Commun.* **1985**, 1618.

0020-1669/93/1332-3727$04.00/0

Table I. Crystal Data for *catena*-(μ-N_3)[Ni(232-tet)](ClO_4) (**1**) and *catena*-(μ-N_3)[Ni(323-tet)](ClO_4) (**2**)

	1	**2**
formula	$[C_7H_{20}N_7Ni]_n(ClO_4)_n$	$[C_8H_{22}N_7Ni]_n(ClO_4)_n$
fw	360.44	374.47
space group	$P2_1/a$	$Pbca$
a, Å	11.806(3)	17.151(2)
b, Å	13.154(3)	16.267(2)
c, Å	9.598(2)	11.478(2)
β, deg	97.90(2)	
V, Å^3	1476(1)	3203(1)
Z	4	8
d_{calc}, g/cm^{-3}	1.621	1.553
μ(Mo Kα), cm^{-1}	15.17	14.03
λ(Mo Kα), Å	0.710 69	0.710 69
T, °C	25	25
scan method	ω-scan	ω-scan
no. of params refined	260	293
R^a	0.045	0.049
$R_w{}^b$	0.055	0.058

^{a} $R(F_o) = \sum||F_o| - |F_c||/\sum|F_o|$. ^{b} $R_w(F_o) = \sum w||F_o| - |F_c||/\sum w|F_o|$.

Table II. Positional Parameters and Equivalent Isotropic Thermal Parameters (Å^2), with Their Estimated Standard Deviations, for *catena*-(μ-N_3)[Ni(232-tet)](ClO_4) (**1**)

atom	x	y	z	$B_{EQ}{}^a$
Ni	0.14280(4)	0.22179(4)	0.25010(5)	2.39(3)
N(1)	–0.0328(3)	0.1770(4)	0.1939(4)	3.80(19)
N(2)	–0.1084(3)	0.2061(3)	0.2514(4)	2.92(16)
N(3)	–0.1813(4)	0.2352(5)	0.3114(5)	4.60(23)
N(4)	0.1025(4)	0.3212(4)	0.4080(5)	3.59(19)
N(5)	0.1646(3)	0.1157(3)	0.4142(4)	3.08(17)
N(6)	0.1863(4)	0.1169(4)	0.1034(5)	3.53(18)
N(7)	0.1288(4)	0.3224(4)	0.0806(5)	3.70(20)
C(1)	0.1404(6)	0.2704(5)	0.5407(6)	4.45(28)
C(2)	0.1077(5)	0.1601(5)	0.5285(6)	4.03(24)
C(3)	0.1307(5)	0.0105(5)	0.3802(7)	4.55(27)
C(4)	0.1864(6)	–0.0324(5)	0.2606(7)	4.46(27)
C(5)	0.1447(6)	0.0111(4)	0.1187(7)	4.48(27)
C(6)	0.1453(6)	0.1622(5)	–0.0368(5)	4.37(26)
C(7)	0.1791(5)	0.2704(5)	–0.0346(6)	4.25(26)
Cl	0.09156(12)	–0.41795(11)	0.24733(18)	4.93(7)
O(1)	0.1907(4)	–0.4784(4)	0.2580(7)	7.61(29)
O(2)	–0.0110(4)	–0.4697(5)	0.2235(7)	8.06(33)
O(3)	0.0923(13)	–0.3425(10)	0.1489(24)	10.24(104)
O(3)′	0.0955(19)	–0.3129(13)	0.2378(33)	6.07(120)
O(3)″	0.1021(20)	–0.4095(25)	0.0813(22)	8.02(127)
O(4)	0.0957(8)	–0.3886(11)	0.3938(11)	18.72(89)

^{a} $B_{EQ} = 8\pi^2/3\sum_i\sum_j U_{ij}a^*_i a^*_j a_i a_j$.

in 10 mL of water. Slow evaporation of the resulting solutions gave violet crystals of the 1-D compounds **1** and **2**, respectively. As previously described,[15] from the mother solution of **1** were simultaneously obtained blue crystals of the ferromagnetic dinuclear complex (μ-N_3)$_2$[Ni(232-tet)]$_2$(ClO_4)$_2$.

The same procedure was followed with the 222-tet and 333-tet, but different results were obtained: by using 222-tet, it was not possible to obtain results analogous to those for **1** or **2**, and by using the 333-tet ligand, the resulting 1-D system was not comparable from the structural and magnetic point of view to the 1-D compounds reported in this paper; this will be the subject of a later publication.

Spectral and Magnetic Measurements. IR spectra were recorded on a Nicolet 520 FTIR spectrophotometer. Magnetic measurements were carried out on a polycrystalline sample with a pendulum type magnetometer (Manics DSM8) equipped with a helium continuous-flow cryostat working in the 4.2–300 K range and a Drusch EAF 16UE electromagnet. The magnetic field was approximately 15 000 G. Diamagnetic corrections (180×10^{-6} cm^3 mol^{-1} for **1** and 224×10^{-6} cm^3 mol^{-1} for **2**) were estimated from Pascal's tables.

Crystal Data Collection and Refinement. Two similar crystals ($0.1 \times 0.1 \times 0.2$ mm) of **1** and **2** were selected and mounted on a Phillips PW-1100 four-circle diffractometer. The crystallographic data, conditions retained for the intensity data collection, and some features of the structure refinement are listed in Table I. The accurate unit-cell parameters were determined from automatic centering of 25 reflections ($8 \le \theta \le 12°$) and refined by least-squares methods. Intensities were collected with graphite-monochromatized Mo Kα radiation, using the ω-scan technique.

For **1**, 2218 reflections were collected in the range $2 \le \theta \le 25°$ ($\pm h, +k, +l$ range), and 2124 reflections were assumed as observed by applying the condition $I \ge 2.5\sigma(I)$. For **2**, 2324 reflections were measured in the range $2 \le \theta \le 25$, 1947 of which were assumed as observed by applying the same condition. In both cases, three reflections were collected every 2 h as orientation and intensity control; significant intensity decay was not observed. Corrections were made for Lorentz–polarization effects but not for absorption. The structures of **1** and **2** were solved by Patterson synthesis using the SHELXS computer program.[16] The two structures were refined by full-matrix least-squares methods, using the SHELX76

Table III. Positional Parameters and Equivalent Isotropic Thermal Parameters (Å^2) with Their Estimated Standard Deviations, for *catena*-(μ-N_3)[Ni(323-tet)](ClO_4) (**2**)

atom	x	y	z	$B_{EQ}{}^a$
Ni	0.08770(3)	0.20009(3)	0.16982(5)	2.64(3)
N(1)	–0.0335(3)	0.1982(4)	0.1892(6)	4.69(26)
C(2)	–0.0751(4)	0.1315(5)	0.1302(8)	5.19(33)
C(3)	–0.0514(5)	0.0490(5)	0.1767(6)	5.49(34)
C(4)	0.0303(4)	0.0232(4)	0.1470(6)	4.63(31)
N(5)	0.0894(3)	0.0727(3)	0.2059(4)	3.31(18)
C(6)	0.1683(4)	0.0444(3)	0.1804(6)	4.26(27)
C(7)	0.2268(3)	0.1087(4)	0.2156(6)	4.43(28)
N(8)	0.2080(3)	0.1846(3)	0.1534(4)	3.22(19)
C(9)	0.2594(4)	0.2533(4)	0.1891(7)	4.92(31)
C(10)	0.2382(4)	0.3306(4)	0.1254(7)	5.19(31)
C(11)	0.1661(5)	0.3721(4)	0.1717(7)	5.05(33)
N(12)	0.0933(3)	0.3280(3)	0.1357(5)	3.85(21)
N(13)	0.0782(3)	0.1734(3)	–0.0159(4)	3.63(20)
N(14)	0.0890(3)	0.2258(3)	–0.0842(4)	3.44(19)
N(15)	0.1018(4)	0.2794(3)	–0.1482(4)	4.76(25)
Cl	–0.1214(1)	0.1008(1)	0.5523(2)	5.16(8)
O(1)	–0.0755(10)	0.1238(15)	0.6611(19)	5.86(73)
O(1)′	–0.1004(11)	0.1154(18)	0.6578(26)	6.95(90)
O(2)	–0.2001(9)	0.1048(20)	0.5597(22)	10.46(135)
O(2)′	–0.1979(18)	0.1409(23)	0.5627(18)	14.28(189)
O(3)	–0.0814(20)	0.1420(17)	0.4517(25)	9.33(115)
O(3)′	–0.0960(21)	0.1466(30)	0.4782(28)	14.82(205)
O(4)	–0.1357(26)	0.0196(18)	0.5321(27)	19.62(254)
O(4)′	–0.0995(17)	0.0166(11)	0.5434(21)	12.36(132)

^{a} $B_{EQ} = 8\pi^2/3\sum_i\sum_j U_{ij}a^*_i a^*_j a_i a_j$.

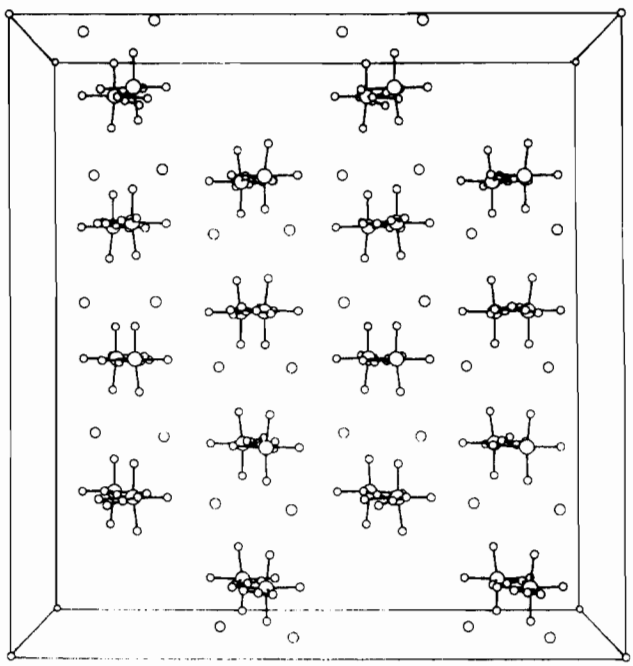

Figure 1. Axial view of four unit cells of compound **2** showing the hexagonal packing of the chains. The same packing is found for all the 1-D compounds referenced in the work. Only nickel, nitrogen, and chlorine atoms are shown for clarity.

(15) Vicente, R.; Escuer, A.; Ribas, J.; Salah el Fallah, S.; Solans, X.; Font-Bardía, M. *Inorg. Chem.* **1993**, *32*, 1920.

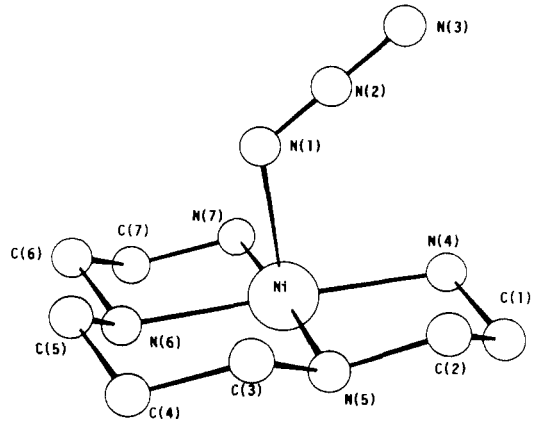

Catena-(μ-N_3)[Ni(232-tet)](ClO_4) (1)

A

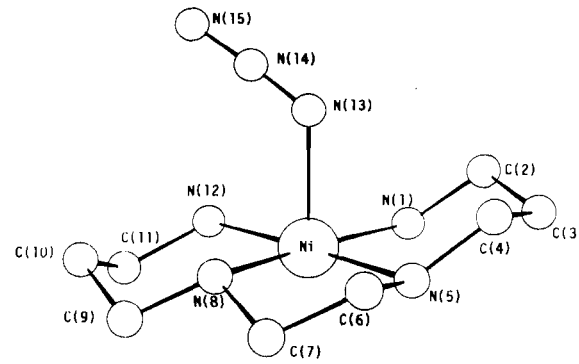

Catena-(μ-N_3)[Ni(323-tet)](ClO_4) (2)

B

Figure 2. Atom-labeling schemes for (A) *catena*-(μ-N_3)[Ni(232-tet)](ClO_4) (**1**) and (B) *catena*-(μ-N_3)[Ni(323-tet)](ClO_4) (**2**).

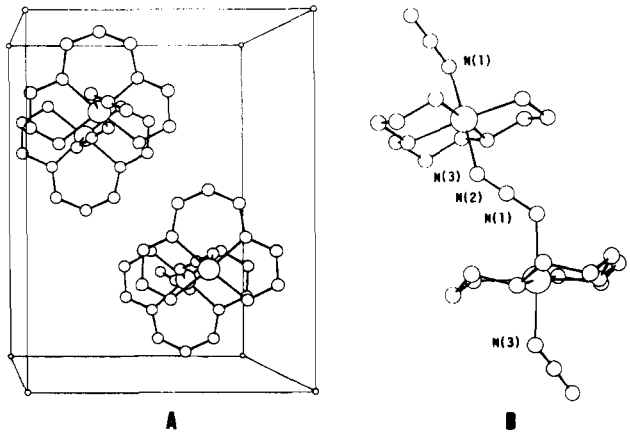

A B

Figure 3. Cell packing for *catena*-(μ-N_3)[Ni(232-tet)](ClO_4) (**1**): (A) axial view clearly showing the torsion between neighboring azido groups (47.4°) and the relative positions of the amino ligands; (B) lateral view showing the non-coplanarity between neighboring Ni–232-tet planes.

computer program.[17] The function minimized was $\sum w[|F_o|-|F_c|]^2$, where $w = (\sigma^2(F_o) + k|F_o|^2)^{-1}$ (k = 0.0063 for **1** and 0.021 for **2**); f, f', and f'' were taken from ref 18. For **1**, oxygen atoms of perchlorate ions were disordered, but only the disordered site of O(3) was obtained from a difference synthesis. All H atom positions were computed and refined with an overall isotropic temperature factor. The final R factor was 0.045 (R_w = 0.055). Number of refined parameters = 260. Maximum shift/esd = 0.1. Maximum and minimum peaks in the final difference synthesis were 0.3 and –0.3 e Å^{-3}, respectively. For **2**, oxygen atoms of perchlorate ions were located in a disorder site; an occupancy factor of 0.5 was assigned according to the height of peaks observed in the Fourier synthesis. All H atoms were located from a difference synthesis and refined with an overall isotropic temperature factor. The final R factor was 0.049 (R_w = 0.058) for all observed reflections. The number of parameters refined was 293. Maximum shift/esd = 0.1. Maximum and minimum peaks in the final difference synthesis were 0.3 and –0.3 e Å^{-3}, respectively. Final atomic coordinates for **1** and **2** are given in Tables II and III, respectively.

Results and Discussion

Description of the Structures. Both structures consist of 1-D nickel–azido chains isolated by ClO_4^- anions found in the interchain space (Figure 1). No hydrogen bonds are present between the chains or between perchlorate groups. In the chain

Table IV. Selected Bond Distances (Å) and Angles (deg) for *catena*-(μ-N_3)[Ni(232-tet)](ClO_4) (**1**)

Distances			
N(1)–Ni	2.151(4)	N(3)′–Ni	2.156(4)
N(4)–Ni	2.107(4)	N(5)–Ni	2.091(4)
N(6)–Ni	2.083(4)	N(7)–Ni	2.087(4)
N(2)–N(1)	1.176(5)	N(3)–N(2)	1.163(6)
Ni–Ni′	5.949(1)		
Angles			
N(4)–Ni–N(1)	92.6(2)	N(5)–Ni–N(1)	91.3(2)
N(5)–Ni–N(4)	83.6(2)	N(6)–Ni–N(1)	88.2(2)
N(6)–Ni–N(4)	176.6(2)	N(6)–Ni–N(5)	93.0(2)
N(7)–Ni–N(1)	90.4(2)	N(7)–Ni–N(4)	99.4(2)
N(7)–Ni–N(5)	176.4(2)	N(7)–Ni–N(6)	83.9(2)
N(2)–N(1)–Ni	124.1(3)	N(2)′–N(3)′–Ni	134.6(3)
N(1)–N(2)–N(3)	178.3(5)		

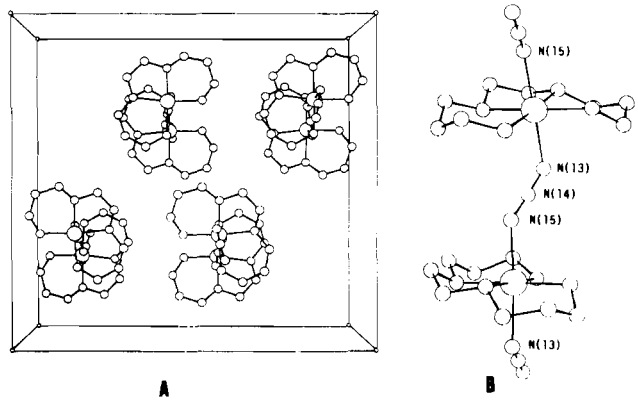

A B

Figure 4. Cell packing for *catena*-(μ-N_3)[Ni(323-tet)](ClO_4) (**2**): (A) axial view showing the torsion between neighboring azido groups (36.5°) and the relative positions of the amino ligands; (B) lateral view showing the non-coplanarity between neighboring Ni–323-tet planes.

structure, each Ni(II) atom is coordinated by one N_4 ligand and two azido ligands in a distorted octahedral *trans* arrangement.

***catena*-(μ-N_3)[Ni(232-tet)](ClO_4) (1).** A labeled diagram and the structure of the cell are shown in Figures 2A and 3A, respectively. The main bond distances and angles are gathered in Table IV. The four nickel–N(232-tet) distances are similar (2.107(4), 2.083(4), 2.091(4), 2.087(4) Å) and shorter than the two nickel–N(azido) distances (2.151(4), 2.156(4) Å), giving an axially elongated octahedron in the chain direction. The four N atoms of the 232-tet ligand and the nickel atom are in the same plane (maximum deviation from the plane 0.019 Å for the nickel atom). The coordination of the azido bridge is asymmetrical: Ni–N(1)–N(2) is 124.1(3)°, Ni–N(3)′–N(2)′ is 134.6(3)°, and the Ni–N_3–Ni torsion angle defined by Ni–N(1)–N(3)–Ni′ atoms

(16) Sheldrick, G. M. *Acta Crystallogr.* **1990**, *A46*, 467.
(17) Sheldrick, G. M. SHELX. A computer program for crystal structure determination. University of Cambridge, England, 1976.
(18) *International Tables for X-ray Crystallography*; Kynoch Press: Birmingham, England, 1974; Vol. IV, pp 99–110, 149.

Table V. Selected Bond Distances (Å) and Angles (deg) for *catena*-(μ-N_3)[Ni(323-tet)](ClO_4) (**2**)

	Distances		
N(1)–Ni	2.091(5)	N(5)–Ni	2.113(4)
N(8)–Ni	2.087(5)	N(12)–Ni	2.120(5)
N(13)–Ni	2.181(4)	N(15)′–Ni	2.129(4)
N(14)–N(13)	1.172(7)	N(15)–N(14)	1.162(6)
Ni–Ni′	5.964(1)		
	Angles		
N(5)–Ni–N(1)	88.8(2)	N(8)–Ni–N(1)	172.2(2)
N(8)–Ni–N(5)	83.4(2)	N(12)–Ni–N(1)	94.5(2)
N(12)–Ni–N(5)	176.5(2)	N(12)–Ni–N(8)	93.3(2)
N(13)–Ni–N(1)	91.5(2)	N(13)–Ni–N(5)	89.8(2)
N(13)–Ni–N(8)	87.8(2)	N(13)–Ni–N(12)	91.1(2)
N(14)–N(13)–Ni	119.8(4)	N(14)′–N(15)′–Ni	135.8(4)
N(13)–N(14)–N(15)	176.9(5)		

Table VI. Structural and Magnetic Parameters for the Five Analogous Systems Compared in This Work

	ligand[a]				
	232-tet	323-tet	cyclam	tmcyclam	tmd
Ni–N(azido), Å	2.151	2.181	2.165	2.150	2.122
	2.156	2.129	2.172	2.150	2.122
Ni–N–N, deg	124.1	119.8	128.2	142.0	120.9
	134.6	135.8	140.7	142.0	120.9
torsion Ni–N_3–Ni, deg	37.6	10.7	13.1	0	0
$\Delta^2(d_{z^2})$	0.130	0.207	0.133	0.085	0.338
J, cm^{-1}	−26.9	−62.7	−39.2	−24.4	−70.0
ref	*b*	*b*	8	13	20

[a] Cyclam is 1,4,8,11-tetraazacyclotetradecane; tmcyclam is 1,4,8,11-tetramethylcyclam; tmd is 1,3-diaminopropane. The complex with tmcyclam is not a 1-D system but a dinuclear one with the same pattern as for the four 1-D chains. [b] This work.

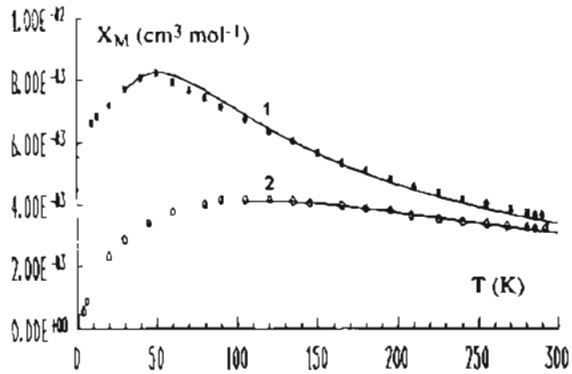

Figure 5. Plots of the magnetic susceptibility vs T for (*) *catena*-(μ-N_3)[Ni(232-tet)](ClO_4) (**1**) and (○) *catena*-(μ-N_3)[Ni(323-tet)](ClO_4) (**2**). Solid lines show the best fit obtained using the Weng equation up to 40 and 105 K, respectively.

is 37.6°. As a consequence of both factors, the angle between the normals to the two neighboring nickel–N_4 232-tet planes is 29.1° (Figure 3B). Between neighboring azido groups there is a torsion angle of 47.4°. As can be seen in Figure 3A, the consecutive 232-tet ligands are turned 180° between them.

***catena*-(μ-N_3)[Ni(323-tet)](ClO_4) (2).** A labeled diagram and the structure of the cell are shown in Figures 2B and 4A, respectively. The main bond distances and angles are gathered in Table V. The four nickel–N(232-tet) distances are 2.091(5), 2.087(5), 2.113(4), and 2.120(5) Å, and the two nickel–N(azido) distances are 2.181(4) and 2.129(4) Å, giving a slightly axially elongated octahedron in the chain direction. The four N atoms of the 323-tet ligand and the nickel atom are in the same plane (maximum deviation from the plane 0.017 Å for N(5)). The coordination of the azido bridge is strongly asymmetrical: Ni–N(13)–N(14) is 119.8(4)°, Ni–N(15)′–N(14)′ is 135.8(4)°, and the Ni–N_3–Ni torsion angle defined by Ni–N(13)–N(15)–Ni′ is 10.7°. As a consequence of both factors, the angle between the normals to the two neighboring nickel–N_4 323-tet planes is 21.6° (Figure 4B). Between neighboring azido groups there is a torsion angle of 36.5°. In contrast to the structure of **1**, the two consecutive 323-tet ligands are turned only 90° between them.

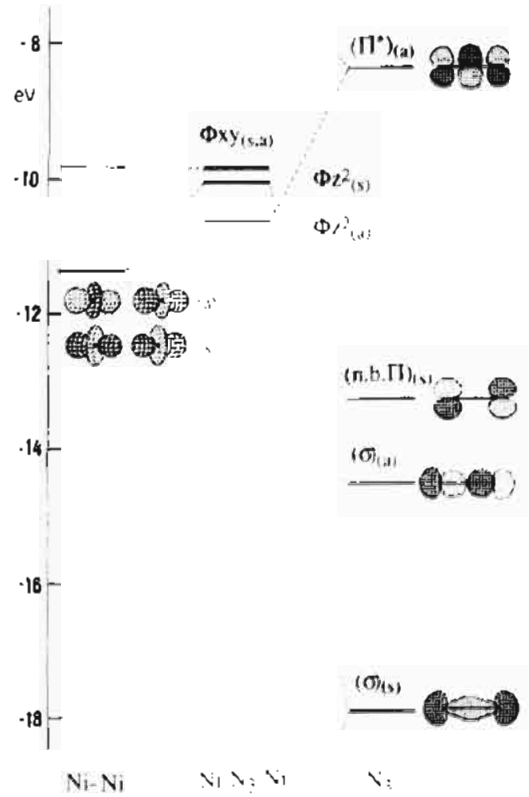

Figure 6. MO diagram for a L_5Ni–N_3–NiL_5 system using the parameters Ni–N–N = 120° and Ni–N_3–Ni torsion = 0°. The significant contributions of azido and Ni–Ni fragments are schematized in the figure.

Magnetic Results. The molar magnetic susceptibilities vs T of *catena*-(μ-N_3)[Ni(232-tet)](ClO_4) and *catena*-(μ-N_3)[Ni(323-tet)](ClO_4) are plotted in Figure 5. The χ_M values (3.69×10^{-3} cm^3 mol^{-1} for **1** and 3.24×10^{-3} cm^3 mol^{-1} for **2**, at room temperature) increase when the temperature decreases, reaching broad maxima ca. 50 K for **1** and ca. 120 K for **2**, with χ_M values of 8.24×10^{-3} cm^3 mol^{-1} for **1** and 4.16×10^{-3} cm^3 mol^{-1} for **2**. For **2**, the χ_M vs T curve decreases continuously and tends to zero at low temperatures, displaying Haldane gap behavior. The positions of the maximum values clearly indicate strong antiferromagnetic coupling between nickel(II) ions through the N_3^- bridge.

Experimental data have been fitted to the Weng equation,[19] based upon the spin Hamiltonian $H = -J\sum S_i S_{i+1}$, where the nickel ion and the nature of the exchange interaction are assumed to be isotropic:

$$\chi_M = (N\beta^2 g^2/kT)(2 + A\alpha + B\alpha^2)/(3 + C\alpha + D\alpha^2 + E\alpha^3)$$

in which $A = 0.019$, $B = 0.777$, $C = 4.346$, $D = 3.232$, $E = 5.834$, and $\alpha = |J|/kT$. Fit is only possible up to near the maximum (in our case up to 40 K for **1**), because neither zero-field splitting nor Haldane gap is taken into account in the equation. Taking into consideration that for **2** the Haldane effect may be operative, fit has been performed up to 105 K. The J value was obtained by minimizing the function $R = \sum(\chi_M^{calcd} - \chi_M^{obs})^2/\sum(\chi_M^{obs})^2$. The best fitting parameters obtained are $J = -26.9$ cm^{-1}, $g = 2.21$, $R = 3.2 \times 10^{-4}$ for complex **1** and $J = -62.7$ cm^{-1}, $g = 2.38$, $R = 1.2 \times 10^{-4}$ for compound **2**.

Magneto–Structural Correlations. In Table VI we present the main structural and magnetic features for **1** and **2**, for two

(19) Weng, C. Y. Ph.D. Thesis, Carnegie Institute of Technology, 1968.

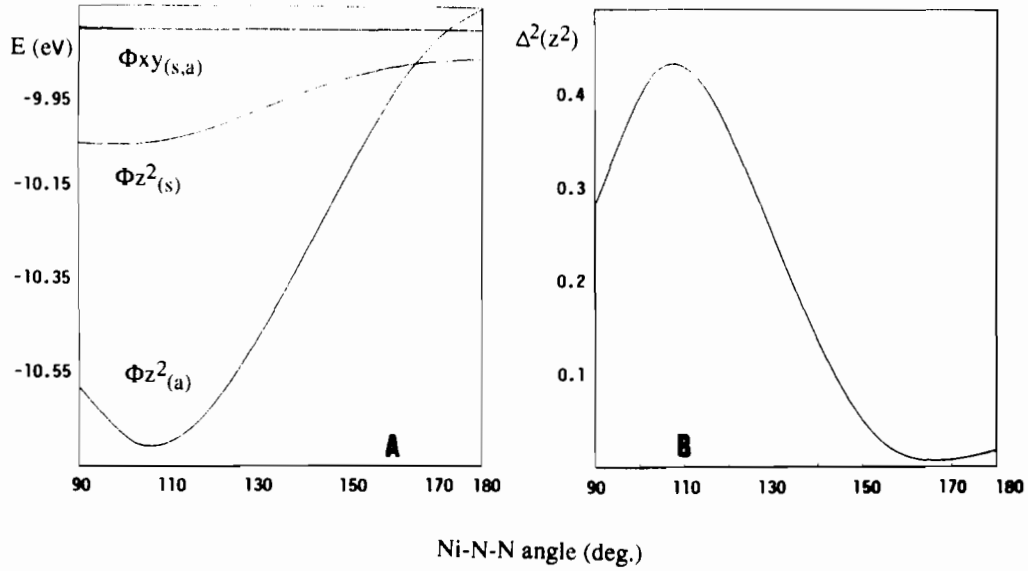

Figure 7. (A) MO correlation diagram for a $L_5Ni–N_3–NiL_5$ system as a function of the variation of the Ni–N–N angle between 90 and 180° with the Ni–N_3–Ni torsion angle = 0°. (B) Plot of the variation of $\Delta^2(z^2)$ vs the Ni–N–N angle from the correlation diagram.

analogous chains previously reported,[8,20] and for one dinuclear system,[12,13] which can be considered as the smallest fragment of a chain.

From Table VI we can realize that all the Ni–N(azido) bond lengths are similar (between 2.12 and 2.18 Å). In contrast, the Ni–NNN bond angles are different (from 119.8° for 323-tet to 142.0° for tmcyclam); the Ni–N_3–Ni torsion angles are also very different (from 0 to 37.6°). The J values are also gathered in Table VI and show a remarkable variation from −24 to −70 cm^{-1}.

In order to establish magneto–structural correlations between these J values and the structural parameters, extended Hückel MO calculations were performed by means of the CACAO program,[21] on a dimeric fragment modeled as follows:

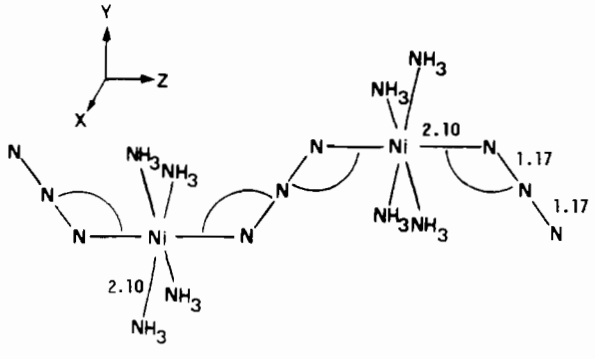

Taking into account that bond distances are similar in all the reported complexes, bond angles may have a significant role in the superexchange interaction between the nickel atoms. We checked the magnitude of this factor by means of MO extended Hückel calculations performed on a simplified dinuclear nickel(II) unit using geometries with the constant distances shown.

Orbital Mechanism of the Interaction through a Single μ-Azido Bridge. For a [NiNi] system the antiferromagnetic component of J is a function[22] of the square of the gaps between xy and z^2 pairs of molecular orbitals. In our case, a [NiNi] system with a single azido bridge in which the Ni–N bridging direction is placed along the z axis, a different role can be expected for the d_{xy} and d_{z^2} orbitals: the xy orbital is roughly perpendicular to the chain direction, and the overlap with the bridge is negligible. These orbitals do not contribute to the exchange mechanism whereas, for z^2 orbitals oriented roughly in the chain direction, the overlap is important and the z direction exchange pathway is operative.

As an example, the calculated MO energy diagram for the Ni–N–N angle of 120° is shown in Figure 6, showing that the two symmetric and antisymmetric MOs with xy contribution ($\varphi xy_{(s)}$ and $\varphi xy_{(a)}$), do not interact with the azido MOs, are degenerated, and do not contribute to the exchange pathway. The $\varphi z^2_{(s)}$ MO receives a contribution from the nonbonding Π and $\sigma_{(s)}$ MOs of the azido group, whereas $\varphi z^2_{(a)}$ has a contribution from the antibonding Π* and $\sigma_{(a)}$ MOs of the azido group. The participation of the terminal N atoms of the azido fragment in the antibonding Π MO is lower than in the other three MOs. Consequently, a lower antibonding character is found in the resulting combinations with the nickel fragment, and $\varphi z^2_{(a)}$ becomes less energetic than $\varphi z^2_{(s)}$.

Effect of the Ni–N–N Angle. The MO correlation diagram for Ni–N–N angles between 90 and 180° (Figure 7A) shows that the energy levels of the xy MOs are constant and equal, the parameter being $\Delta^2(xy) = |E(\varphi xy_{(s)}) - E(\varphi xy_{(a)})|^2 = 0$, whereas the energies E of z^2 MOs show a strong variation: the $E(\varphi z^2_{(s)})$ level is practically constant, but the $E(\varphi z^2_{(a)})$ one is strongly dependent on the bond angle. The value of $\Delta^2(z^2) = |E(\varphi z^2_{(s)}) - E(\varphi z^2_{(a)})|^2$ vs Ni–N–N angle, shown in Figure 7B, has a maximum at 108° and is zero at 164°. According to the Hoffmann model,[22] $J_{AF} \propto \Delta^2(z^2) + \Delta^2(xy)$, the strongest antiferromagnetic coupling is foreseen to be for angles near 110°, and for larger angles, the J parameter must decrease quickly. For very high values of this Ni–N–N angle, even ferromagnetic behavior can be expected, but azido bridges with this bond angle are experimentally improbable.

To explain this exchange mechanism in a qualitative way, drawings of the φz^2 MOs at several selected Ni–N–N angles are useful (Figure 8). As shown in the figure, for angles close to 90°, the exchange pathway occurs mainly through the Π system of the azido group whereas, for angles close to 180°, the exchange pathway occurs mainly through the σ system. With the experimentally observed angles (120–140°), a mixture of both pathways is produced. For $\varphi z^2_{(s)}$, the antibonding interaction is practically constant, giving an almost constant energy level. In contrast, for $\varphi z^2_{(a)}$, a large antibonding interaction is obtained at

(20) Gadet, V.; Verdaguer, M.; Renard, J. P.; Ribas, J.; Monfort, M.; Diaz, C.; Solans, X.; Landee, C. P.; Jamet, J. P.; Dworkin, A. *J. Am. Chem. Soc.*, in press.
(21) Mealli, C.; Proserpio, D. M. *J. Chem. Educ.* **1990**, *67*, 3399.
(22) Hay, P. J.; Thibeault, J. C.; Hoffmann, R. *J. Am. Chem. Soc.* **1975**, *97*, 4884.

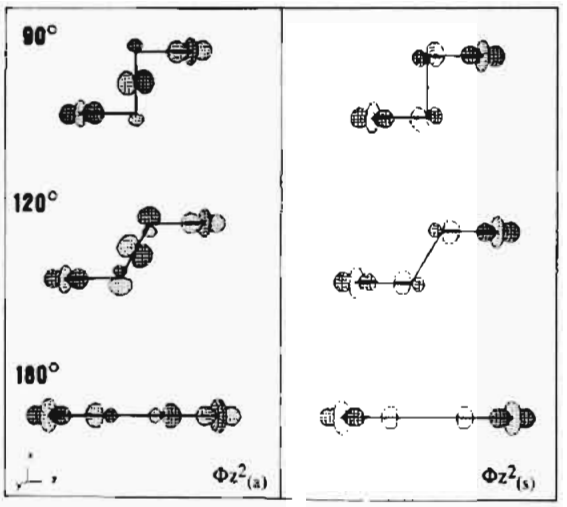

Figure 8. Plot of the selected dz^2 (s, a) MOs showing the main σ (180°) and Π (90°) superexchange pathway. For experimental angles placed between 120 and 140°, the superexchange pathway is a mixture of both contributions.

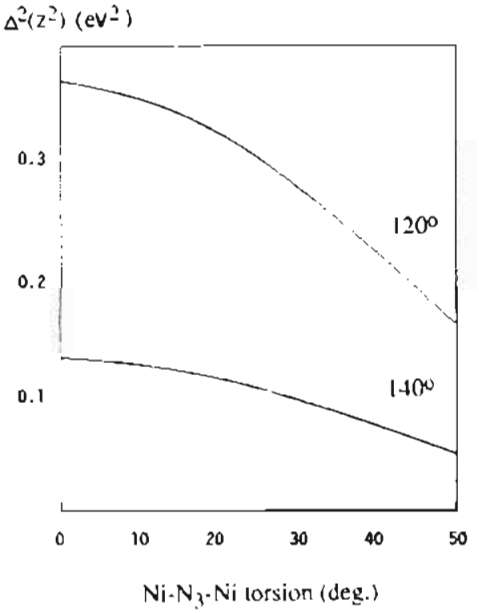

Figure 9. Plot of the variation of $\Delta^2(z^2)$ vs the Ni–N_3–Ni torsion angle between 0 and 50° for a L_5Ni–N_3–NiL_5 system, for fixed Ni–N–N angles of 120 and 140°.

large angles, since this antibonding interaction is greater with the σ MO than with the Π MO of the azido group.

Effect of the Ni–NNN–Ni Torsion Angle. The influence of the Ni–N_3–Ni torsion angle on the antiferromagnetic coupling was previously pointed out by Hendrickson,[23] using symmetry arguments. Results of MO extended Hückel calculations at fixed Ni–N–N angles (120 and 140°) with variable Ni–N_3–Ni torsion angles (0–50°) show (Figure 9) that $\Delta^2(z^2)$ is almost constant between 0 and 10° but decreases at higher values: the $\Delta^2(z^2)$ value at 50° is roughly 40% of the value at 0°. The strongest antiferromagnetic coupling is thus expected for Ni–N_3–Ni torsion angles close to zero for a fixed Ni–N–N angle.

Checking the Experimental Data. To check the above conclusions, we use the data reported in Table VI. The main

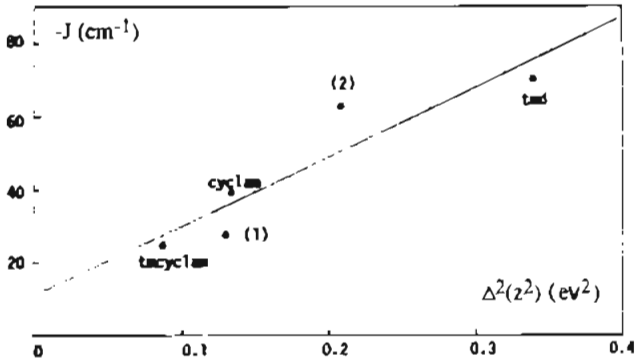

Figure 10. Plot of the experimental $-J$ values vs calculated $\Delta^2(z^2)$ using the parameters in Table VI.

experimental features can be summarized as follows: (i) For the simplest cases, for large Ni–N–N angles, even with low Ni–N_3–Ni' torsion, $|J|$ is weak (tmcyclam), and for weak Ni–N–N and low Ni–N_3–Ni' torsion, $|J|$ is strong (tmd). (ii) When the two angular effects are conflicting, a more complex situation arises and intermediate values of J are obtained. Nevertheless, the comparison of J values for couples of compounds, when one of the two angles is constant, allows us to verify the main conclusions of the calculations. (iii) This is also the case when the true geometries are used in the calculation of $\Delta^2(z^2)$ (Figure 10).

Concluding Remarks

Several years ago, Kahn and co-workers[24] pointed out that the so-called spin polarization model may describe more correctly the superexchange coupling for the azido ligand: "in particular, the ferromagnetic interaction observed in EO azido-bibridged copper(II) dimers cannot be explained in a satisfactory way by the accidental orthogonality of the magnetic orbitals". According to them, the MO qualitative models did not allow one to rationalize the experimental data. Some of the authors recently reported a tetranuclear nickel(II) complex with an EO azido bridge,[25] for which the spin polarization seems necessary to explain the ferromagnetic behavior. On the contrary, Bencini and co-workers[26] have rationalized their results for cobalt(II) and nickel(II) dinuclear complexes with end-to-end azido bridges with EH calculations. In this work we have also attempted to correlate our results with MO extended Hückel calculations, with good agreement. Our results seem indicate that EH calculations are appropriate, at least, for end-to-end azido bridges.

Acknowledgment. This work was financially supported by the CICYT (Grant PB91/0241).

Supplementary Material Available: Tables of complete crystal data, anisotropic thermal parameters, hydrogen atom coordinates, angles, and distances for *catena*-(μ-N_3)[Ni(232-tet)](ClO_4) (**1**) and *catena*-(μ-N_3)-[Ni(323-tet)](ClO_4) (**2**) (13 pages). Ordering information is given on any current masthead page.

(23) Duggan, M. D.; Barefield, E. K.; Hendrickson, D. N. *Inorg. Chem.* **1973**, *12*, 985.
(24) Charlot, M. F.; Kahn, O.; Chaillet, M.; Larrieu, C. *J. Am. Chem. Soc.* **1986**, *108*, 2574.
(25) Ribas, J.; Monfort, M.; Costa, R.; Solans, X. *Inorg. Chem.* **1993**, *32*, 695.
(26) Bencini, A.; Ghilardo, C. A.; Midollini, S.; Orlandini, A. *Inorg. Chem.* **1989**, *28*, 1958.